DALTON
FULL PAPER

Structural studies and matrix photochemistry of tetramethyloxorhenium(VI), $(CH_3)_4ReO$, and related compounds

Leigh J. Morris,[a] Anthony J. Downs,[a] Jennifer C. Green,[a] Tim M. Greene,*[b] Simon J. Teat[c] and Simon Parsons*[d]

[a] *Inorganic Chemistry Laboratory, University of Oxford, South Parks Road, Oxford, UK OX1 3QR*
[b] *School of Chemistry, University of Exeter, Stocker Road, Exeter, UK EX4 4QD. E-mail: tmgreene@ex.ac.uk*
[c] *CLRC Daresbury Laboratory, Warrington, Cheshire, UK WA4 4AD*
[d] *Department of Chemistry, University of Edinburgh, West Mains Road, Edinburgh, UK EH9 3JJ*

Received 8th March 2002, Accepted 10th June 2002
First published as an Advance Article on the web 17th July 2002

The crystal structure of tetramethyloxorhenium(VI), $(CH_3)_4ReO$, **1**, at 150 K reveals molecules with a square-based pyramidal skeleton and dimensions very similar to those in the gas phase. The related binuclear compound $[(CH_3)_3Re(O)]_2O$, **2**, has likewise been shown to feature rhenium centres with a similar coordination geometry linked by a linear Re–O–Re bridge and carrying terminal Re=O bonds that are mutually *trans*. Salient average dimensions (distances in Å, angles in °) are as follows: **1** Re–C 2.110(8), Re=O 1.684(4), O=Re–C 112.6(2), C–Re–C 81.5(5) and 134.8(3); **2** Re–C 2.095–2.134(11), Re=O 1.675(6), Re–O 1.851(1), O=Re–C 103.0–113.5(4), C–Re–C 79.2(4) and 132.5–137.0(4). Density functional theory (DFT) calculations have been performed to predict ionization energies for $(CH_3)_4ReO$. In the light of these results, the photoelectron spectrum has been reassigned. IR spectroscopic measurements have been used to chart the reactions activated by irradiating solid argon matrices doped with **1** with broad-band UV-visible light ($200 \leq \lambda \leq 800$ nm). The spectra have been interpreted on the basis of additional experiments with $(CD_3)_4ReO$, **1**-d_{12}, and by comparison either with the vibrational properties forecast by calculations or with those of known related molecules. Hence photoexcitation is shown to result in the elimination of methane and the formation of the novel methylidene–rhenium(VI) compound $H_2C{=}Re(O)(CH_3)_2$, **3**. The results are discussed in relation to the photochemistry of methyltrioxorhenium(VII) in similar circumstances.

The first sighting of an alkyl oxo rhenium compound was reported in 1974 by Wilkinson and co-workers.[1] Interaction of methyllithium with the Re(V) complex $[Re(O)Cl_3(PPh_3)_2]$ in the presence of traces of oxygen was then shown to yield tetramethyloxorhenium, $(CH_3)_4ReO$, **1**, as a deep purple, crystalline solid that was characterised by its IR and mass spectra. With a melting point of 44 °C, the solid sublimes very readily *in vacuo* at room temperature and, although very sensitive to attack by O_2 and NO, it is thermally robust, surviving in the gas phase at temperatures up to 150 °C.

Interest in such alkyl oxo rhenium compounds has been stimulated by the wide range of catalytic activity exhibited by what is now the best known representative, namely methyltrioxorhenium(VII), CH_3ReO_3.[2,3] This has led to extensive research into the physical and chemical properties of not only CH_3ReO_3 itself, but also related compounds, such as $C_2H_5ReO_3$,[4] $(CH_3)_3ReO_2$,[5] and $(CH_3)_4Re_2O_4$.[6] Apart from the original studies by Wilkinson and co-workers,[1,7–9] which included an assignment of the photoelectron spectrum of **1**, little has been heard of the rhenium(VI) compound, **1**. Only recently have electron-diffraction measurements established a square-pyramidal skeleton with C_{4v} symmetry for the gaseous $(CH_3)_4ReO$ molecule.[10]

Here we report the results of crystallographic and computational studies carried out on **1** and of crystallographic studies carried out on its binuclear derivative $[(CH_3)_3Re(O)]_2O$, **2**, formed by inadvertent but limited exposure of **1** to moist air. In addition, we have investigated the photochemistry of **1** by reference to the IR spectrum of the molecules isolated in a solid argon matrix at low temperatures. Hence it will be shown that CH_4 is eliminated with the formation of the novel methylidene rhenium(VI) compound $H_2C{=}Re(O)(CH_3)_2$, **3**, in a reaction which contrasts with the tautomerisation of CH_3ReO_3 to give $H_2C{=}Re(O)_2OH$ under similar conditions.[11] The identification of **3** on the basis of its IR spectrum has been endorsed (i) by the response to perdeuteriation of the precursor **1**; (ii) by comparison of the wavenumbers and intensities in IR absorption with those deduced by density functional theory (DFT) calculations; and (iii) by analogies with the spectra of related methylidene and Re=O derivatives, *e.g.* MCH_2 (M = Cr, Mn, Co, Ni or Cu),[12] $H_2C{=}Re(O)_2OH$,[11] and $OReF_4$.[13] Some consideration is given to the likely mechanisms of the reactions leading from **1** to **2** and from **1** to **3**.

Experimental

Synthesis

Tetramethyloxorhenium(VI), **1**, was synthesised from $[Re(O)Cl_3(PPh_3)_2]$ and CH_3Li (1.4 M solution in Et_2O, ex Aldrich) according to the method described previously.[7] After slow evaporation of the Et_2O solvent at 233 K, the residue was vaporised *in vacuo* and the vapour fractionated through a series of traps held successively at 231, 195 and 77 K. Purple solid **1** collected in the first trap and was authenticated by its IR spectrum measured for a thin film of the annealed condensate formed at 77 K. Yields were typically about 60% based on the quantity of $[Re(O)Cl_3(PPh_3)_2]$ taken, but were often much reduced by some codistillation of the product during evaporation of the ether solvent. Samples of the perdeuteriated com-

 DOI: 10.1039/b202425j

pound, $(CD_3)_4ReO$, **1**-d_{12}, were prepared in a similar way with CD_3Li (0.5 M solution of CD_3Li/LiI in Et_2O, ex Aldrich) being used in place of CH_3Li.

Growth of crystals for X-ray diffraction

A sample of **1** was kept under vacuum in a Pyrex glass ampoule that was closed by a Young's Teflon-seated tap. After several days at room temperature, crystals of an appropriate size were observed to have formed by sublimation on to the walls of the vessel. A single crystal was selected for study at 150 K by diffraction of silicon-monochromated synchrotron radiation ($\lambda = 0.6886$ Å), data being collected on a Bruker SMART three-circle CCD-diffractometer on Station 9.8 at Daresbury Laboratory.[14] Earlier attempts to solve the crystal structure of **1** using several data sets collected at Edinburgh on a Stoë Stadi four-circle diffractometer with a conventional Mo-Kα source failed to reach satisfactory convergence, with *R*-factors in the range 5–7% and difference map maxima exceeding 5 e Å^{-3}. The source of these difficulties remains unresolved, but, with cell dimensions in the approximate ratios 2 : 1 : 2, it is possible that the samples suffered from a small amount of secondary twinning based on a metrically cubic supercell. Use of synchrotron radiation enabled a very much smaller crystal to be studied than is possible with conventional equipment, and it seems quite possible that secondary twinning was simply avoided under these conditions. Optical microscopy made it clear that the crystal finally used for data collection had no attached 'passengers' or re-entrant angles, although this procedure could not be applied to the larger crystals because of their intense colour.

After a period of several weeks of containment in an evacuated Pyrex glass ampoule, certain samples were observed to undergo a colour change from deep purple to bright red–orange. The new material so produced was an involatile crystalline solid that did not appear to engage in any further reactions once formed. A single crystal was selected for study at 150 K by X-ray diffraction using a Stoë Stadi four-circle diffractometer with a conventional Mo-Kα source. Hence the bright red–orange plates were identified as the binuclear rhenium(VI) compound $[(CH_3)_3Re(O)]_2O$, **2**.

Crystallography: data collection, structure solution and refinement

Details of the data and data collection for crystals of the compounds **1** and **2** are given in Table 1.

(a) Complex 1

An absorption/decay correction based on equivalent data was applied using SADABS.[15] Of the 9196 data with $F > 4\sigma(F)$ measured, 1496 were unique ($R_{int} = 0.078$); 1298 data with $F > 4\sigma(F)$ were used in all calculations. Anomalous dispersion terms f' and f'' were calculated using the program FPRIME.[16]

Although the unit cell of **1** is metrically tetragonal, general data in parity groups (*gug*) and (*ugu*) were systematically absent. This was initially interpreted as being diagnostic of an orthorhombic A- or C-centred crystal twinned by a four-fold rotation about the *b* (5.55 Å) axis. Identification of a clear *c*-glide perpendicular to the *b* axis suggested *Cmcm* as the initial choice of space group.

The structure was solved from the Patterson function,[17] which contained a dominant peak at [0, 0.77, 1/2], placing the Re on an *m2m* special position. The four-fold axis which forms the twin law can be expressed by the matrix (001/010/−100), and, when considered with the C-centring conditions, this makes it clear that reflections with $h + k = 2n$ and $k + l = 2n$ will contain contributions from both twin elements: those with $h + k = 2n$ and $k + l \neq 2n$ are contributed only by twin component 1, and those with $h + k \neq 2n$ and $k + l = 2n$ arise only from component 2. The (*gug*) and (*ugu*) reflections will always be absent, and these were removed from the data set. While the oxygen atom was located readily in a difference synthesis calculated on this basis, the C atoms were disordered by the two crystallographic mirror planes.[18] The space group was therefore reduced to *C*2/*c* which permits an ordered description of the structure to be given.

The coordinates of the two carbon atoms are closely related, *viz.* $x(Cl) + z(Cl) \approx 1/2$, $x(C2) \approx z(C2)$ and $y(Cl) \approx y(C2)$, and free refinement of the model revealed correlations between positional parameters of these atoms. The displacement parameters were also correlated, and this may have been responsible for the rather implausible differences in the carbon anisotropic displacement parameters and Re–C bond lengths which developed on free refinement. Following the strategies for controlling refinement under these circumstances devised by Watkin,[19] the model was reparameterised so that the six C-positional parameters were refined as $x(Cl) \pm z(Cl)$, $x(C2) \pm z(C2)$, and $y(Cl) \pm y(C2)$. The anisotropic displacement parameters (adps) were similarly combined on the assumption that they are related by the molecular four-fold axis [*i.e.* $U_{11}(C1) \pm U_{33}(C2)$ *etc.*]. Similarity restraints were applied to Re–C and C–O distances, and to adp components related by the molecular four-fold axis [*e.g.* the sum $\{U_{23}(C1) + U_{12}(C2)\}$ was restrained to zero]. Hydrogen atoms were placed in calculated positions *anti* to the Re=O bond and assigned isotropic displacement parameters equal to $1.5U_{eq}$[C]. The refinement (against *F*) converged to $R = 3.79\%$, $R_w = 3.75\%$, and $S = 1.0277$ with 30 parameters, 10 restraints, and a Chebychev 3-term polynomial weighting scheme. There were no correlation coefficients greater than 0.8, and the twin components refined to 0.647(1) and 0.353(1). The final difference synthesis showed a maximum of +1.63 e Å^{-3} and a minimum of −2.00 e Å^{-3}, both next to the Re atom. These are attributable to residual absorption errors; a difference map calculated using the same weighting scheme as in the refinement showed extrema of +1.19 and −1.26 e Å^{-3}, implying that the reflections affected most strongly by absorption errors were down-weighted by the Chebychev weighting scheme.

(b) Complex 2

Crystal data for **2** were collected at 150 K on a Stoe Stadi-4 diffractometer equipped with an Oxford Cryosystems low-temperature device. The crystal was an orange plate developed in (001); an absorption correction was applied by Gaussian integration following refinement of the crystal shape and dimensions against a set of Ψ-scans. In addition, 176 data for which either the incident or diffracted beams made an angle with the plate face of less than 2° were omitted from the refinement as these are most susceptible to residual absorption errors. The structure was solved using Patterson methods (DIRDIF)[20] and refined by full-matrix least squares against F^2.[16] H atoms were placed using the Sheldrick 'circular Fourier' procedure; all non-H atoms were modelled with adps. The conventional *R*-factor [based on *F* and 2559 data with $F > 4\sigma(F)$] converged to 2.99%; other refinement parameters are given in Table 1.

A disordered crystal structure of this compound has been previously determined by Hursthouse *et al.* using room temperature data.[21] Our cell has a volume approximately three times that of Hursthouse's cell, and there was a systematic weakness in our data set for reflections with $h + 2k \neq 3n$, which had a mean $I/\sigma = 16.2$ compared with 26.3 for the remainder of the data. This information was used to derive Hursthouse's original setting by means of the transformation

$$\begin{pmatrix} 1/3 & -1/3 & 0 \\ 2/3 & 1/3 & 0 \\ 2/3 & 1/3 & 1 \end{pmatrix}.$$

Application of the transpose of the inverse of this matrix, followed by inversion and an origin shift of (1/2, 1/2, 1/2) to our

Table 1 Crystal data, data collection and structure refinement for **1** and **2**

	1	**2**
Empirical formula	$C_4H_{12}ReO$	$C_6H_{18}O_3Re_2$
Formula weight	262.34	510.60
Habit	Red needle	Orange plate
Size/mm	0.14 × 0.02 × 0.02	0.39 × 0.16 × 0.06
Crystal system	Monoclinic	Triclinic
Space group	*C*2/*c*	*P*-1
a/Å	10.922(4)	9.961(4)
b/Å	5.5519(18)	9.967(4)
c/Å	10.894(4)	10.608(5)
α/°	90	107.79(2)
β/°	90.090(7)	110.99(2)
γ/°	90	99.54(2)
T/K	150	150
Volume/Å^3	660.6	890.2
Z	4	3
μ/mm^{-1}	16.82	20
Range of transmission	0.500–0.802	0.145–0.615
Unique data used in refinement/total unique	1298/1496	3003/3003
R_1	3.79[a]	2.99[a]
R_w	3.75[b]	6.03[b]
S	1.028	1.036
Difference synthesis max. and min./e Å^{-3}	1.63, −2.00	+1.37, −1.65
Number of parameters	30	161

[a] Based on *F* and data with $F > 4\sigma(F)$. [b] Based on F^2 and all data.

Re positions recovers approximately Hursthouse's metal coordinates, so that the low temperature structure reported here can largely be considered to be derived from the room temperature structure by ordering of the ligands following an order–disorder phase transition.

CCDC reference numbers 181357 and 181358.

See http://www.rsc.org/suppdata/dt/b2/b202425j/ for crystallographic data in CIF or other electronic format.

Matrix isolation studies

The vapour over a sample of **1** held at 248 K was codeposited continuously with an excess of argon on a CsI window cooled to 16 K by means of a Displex closed-cycle refrigerator (Air Products model CS 202); fuller details of the apparatus are given elsewhere.[22] Typical deposition rates of matrix gas were *ca.* 3 mmol h^{-1}, continued over a period of 2 h. Following deposition and IR analysis of the resulting matrix, the sample was exposed to broad-band UV-visible radiation ($200 \leq \lambda \leq 800$ nm). The photolysis source was a Spectral Energy Hg–Xe arc lamp operating at 800 W and the output from which was invariably limited by a water filter to absorb IR radiation and so minimise any heating effects. Experiments were also carried out to determine the effects of using Oriel high-energy band pass filters in order to irradiate the matrix with either visible light ($400 \leq \lambda \leq 800$ nm) or UV light ($200 \leq \lambda \leq 400$ nm).

IR spectra of the matrix samples were recorded over the range 4000–400 cm^{-1} with a Nicolet 'Magna' 560 FT-IR spectrometer. Measurements were made typically at a resolution of 0.5 cm^{-1} and with an accuracy of ±0.1 cm^{-1}.

Computational methods

Density functional calculations were carried out using the Amsterdam Density Functional code (ADF 2000.2).[23] The basis set used triple-ζ accuracy sets of Slater-type orbitals with relativistic corrections, with a single polarisation functional added to the main group atoms. The cores of the atoms were frozen [C and O(1s), Re(4d)]. The GGA (non-local) method was followed, using Vosko, Wilk and Nusair's local exchange correlation[24] with non-local exchange corrections by Becke[25] and non-local correlation corrections by Perdew.[26,27] Vertical ionisation energies were estimated for the optimised structure from the difference between the total energy of the molecule and that of the molecular ion in the appropriate state. Convergence was most readily achieved for the ion states when the input basis function for the SCF calculation comprised the MOs of the molecular calculation. This also enabled a ready check on how precisely the 'hole' in the ion could be described as a single MO in the molecule.

Table 2 Bond lengths/Å and angles/° for crystalline $(CH_3)_4ReO$, **1**, together with the corresponding measurements made by gas-phase electron diffraction and DFT calculations

	Single crystal[a]	Gas phase[b]	Calc.[c]
Re(1)–O(1)	1.684(4)	1.682(3)	1.703
Re(1)–C(1)	2.113(8)	2.117(3)	2.138
Re(1)–C(2)	2.107(8)		
O(1)–Re(1)–C(1)	112.53(14)	112(1)	112
O(1)–Re(1)–C(2)	112.70(14)		
C(1)–Re(1)–C(2)	81.8(5)	82(1)	82
C(1)#1–Re(1)–C(2)	81.2(5)		
C(2)–Re(1)–C(2)#1	134.6(3)	136(4)	136
C(1)–Re(1)–C(1)#1	134.9(3)		

[a] Symmetry transformations used to generate equivalent atoms: #1 $-x$, y, $-z + 1/2$. [b] See ref. 10. [c] See text for details of the calculations.

Fragment analyses were carried out on $(CH_3)_4ReO$. This involved single point calculations using the MOs of the Re, O and CH_3 fragments as the basis set for the molecular calculations. The fragments retain the geometries found for the optimised molecular structure.

Linear transit calculations stepped a single interatomic distance between fixed values while optimising the remaining atomic coordinates.

The total energies of molecules are referenced in ADF to spin-averaged neutral atoms, in which the electron density is equal in any set of degenerate orbitals. They do not necessarily correspond to the atomic ground states.

Results and discussion

Crystal structure of tetramethyloxorhenium(VI), 1, at 150 K

Crystalline **1** is composed of more or less discrete $(CH_3)_4ReO$ molecules illustrated in Fig. 1 with the bond lengths and angles listed in Table 2. Hence it is apparent that the square-based pyramidal geometry and dimensions of the C_4ReO skeleton

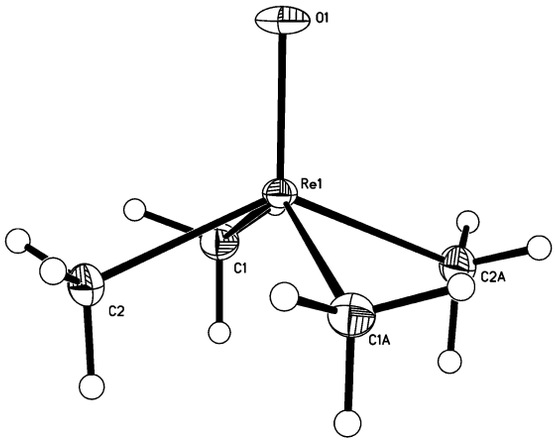

Fig. 1 Structure of $(CH_3)_4ReO$, **1**, as determined by X-ray diffraction of a single crystal at 150 K. Ellipsoids are drawn at the 30% probability level.

match closely those deduced on the basis of the electron-diffraction pattern of the gaseous molecule.[10] The weakness thus implied for the intermolecular forces in the solid is also consistent with the volatility of the material at ambient temperatures. In this respect, **1** resembles $OReCl_4$, the crystal structure of which[28] is also made up of square-pyramidal monomers with local C_{4v} symmetry and little different from the gaseous molecule,[29] with only very weak Re–Cl ··· Re interactions between these units. The low melting point of $OReCl_4$ (303 K) then stands in stark contrast to that of $OWCl_4$ (503 K), crystals of which consist of $OWCl_4$ units linked through *strong*, asymmetric W–O–W bridges into endless chains.[30]

At 2.110(8) Å the average Re–C distance in **1** is slightly longer than that in CD_3ReO_3 [2.063(2) Å], as determined by neutron diffraction studies of a powder sample,[31] and marginally shorter than that in $(CH_3)_6Re$ [2.125(6) Å], as determined by single-crystal X-ray diffraction measurements.[32] This is in accord with both the degree of saturation and the oxidation state of the metal centre. The corresponding Os–C distance in the structural analogue $(CH_3)_4OsO$, determined by electron diffraction of the gaseous molecule, is, as expected for the smaller metal centre, just slightly shorter [2.096(3) Å].[33] Conversely, rather longer M–C bonds measuring 2.180(5) and 2.146(3) Å are found, again by electron diffraction, in gaseous $(CH_3)_5Ta$[34] and $(CH_3)_6W$,[35] respectively.

The other dimensions are unsurprising. The Re=O bond measuring 1.684(2) Å is, within experimental error, metrically identical with the Os=O bond [1.681(4) Å] in $(CH_3)_4OsO$,[33] if slightly shorter than the Re=O bonds [1.702(1) Å] in the rhenium(VII) compound CH_3ReO_3.[30] An equally close level of agreement is found between the rather wide O=M–C angles in $(CH_3)_4ReO$ [112.53(14)°] and $(CH_3)_4OsO$ [112.2(5)°]. Further comparison of the average C–M–C_{cis} angle of 81.5(5)° in crystalline **1** with those in the molecules $(CH_3)_4OsO$ [81.8(4)°][33] and $(CH_3)_5Ta$ [82.2(9)°][34] confirms the trend first noted by Haaland *et al.*[10] that transition metals of the sixth period favour a value near 82° for this parameter.

Crystal structure of $[(CH_3)_3Re(O)]_2O$, 2, at 150 K

The binuclear methylrhenium(VI) oxide $[(CH_3)_3Re(O)]_2O$, **2**, is not a new compound. It was in fact reported in 1985 by Wilkinson *et al.*, having been prepared in high yield by the reaction of $(CH_3)_3SiOReO_3$ with trimethylaluminium in hexane solution.[21] An X-ray diffraction study of the compound at that time was hampered by extensive disorder, and must have been a considerable undertaking given the facilities available at the time.[21] Our low-temperature study revealed an ordered structure allowing us to secure a more precise definition of the molecular geometry.

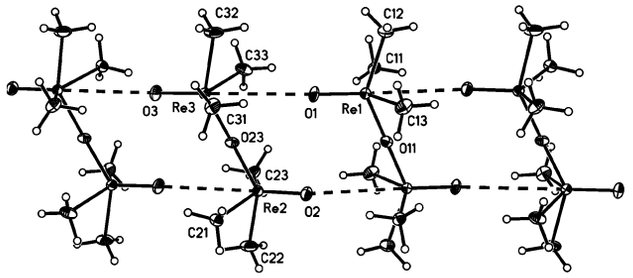

Fig. 2 Structure of $[(CH_3)_3Re(O)]_2O$, **2**, as determined by X-ray diffraction of a single crystal at 150 K showing the presence of strands in the solid state; the long Re–O contacts (shown as dashed lines) are Re1–O2 3.383(8), Re2–O3 3.499(9) and Re3–O1 3.627(8) Å. Ellipsoids are drawn at the 30% probability level.

The crystal structure of **2** is illustrated in Fig. 2. The analysis revealed the presence of two crystallographically distinct molecules in the unit cell. As is often the case for penta-coordinated systems, it is possible to describe the coordination environment of the metal in terms of either a distorted square pyramidal or a distorted trigonal bipyramidal geometry. Thus, both crystallographic molecules of $[(CH_3)_3Re(O)]_2O$ contain two rhenium centres each set below the pseudobasal plane of what may be regarded as a distorted square-based pyramid with the unique Re=O bond at the apex. The two metal centres are linked through a common pseudobasal O atom by a linear Re–O–Re bridge with the Re=O apices oriented *trans* to each other. The structure is thus comparable with that adopted by the (trimethylsilyl)methyl derivative $\{[(CH_3)_3SiCH_2]_3Re(O)\}_2O$.[21] An alternative view would place each Re atom at the centre of a distorted trigonal bipyramid with two CH_3 groups and the terminal O atom forming what approximates to an equatorial plane. The remaining CH_3 group and bridging O atom would then be located in the pseudoaxial positions, but with the resulting C–Re–O unit bent away from the equatorial Re=O bond.

Selected bond lengths and angles for $[R_3Re(O)]_2O$ molecules [R = CH_3 or $(CH_3)_3SiCH_2$[21]], together with the corresponding parameters for the gaseous mononuclear rhenium(VII) molecule $(CH_3)_3ReO_2$,[5] are presented for comparison in Table 3. There is little variation in the Re=O distances which span the range 1.675(6) Å in $[(CH_3)_3Re(O)]_2O$ to 1.703(3) Å in $(CH_3)_3ReO_2$,[5] and still less in the bridging Re–O bonds in the two binuclear compounds [1.851(6) and 1.856(5) Å for R = CH_3 and $(CH_3)_3SiCH_2$,[21] respectively].

The molecule $(CH_3)_3ReO_2$ can be described as having a distorted trigonal bipyramidal structure (although an edge-bridged tetrahedron[36] might be a more appropriate description) with a pseudoaxial C–Re–C unit bent towards the unique pseudo-equatorial CH_3 group such that $<C_{ax}–Re–C_{ax}$ = 146.9(22)°.[5] This compares with the corresponding C–Re–O angles in $[R_3Re(O)]_2O$ molecules which range from 140.0(3)° (**2**, molecule **I**) and 141.8(4)/143.1(4)° (**2**, molecule **II**) to 137.6(1)° in $\{[(CH_3)_3SiCH_2]_3Re(O)\}_2O$.[21] By contrast, the C–Re–C bond angles take on values that fall in two ranges, *viz.* (i) 73.5–80.4° and (ii) 132.5–146.9° [*cf.* 81.5 and 134.8° in $(CH_3)_4ReO$]. The variations of angular geometry, which undoubtedly reflect the influence of make-up and bulk of the ligand environment, serve merely to emphasise the difficulty of assigning the geometric parentage of this environment to either a square-based pyramid or a trigonal bipyramid.[5]

Electronic structure of 1

The electronic structure of the optimised $(CH_3)_4ReO$ was subjected to an orbital analysis. The frontier orbitals, their energies and compositions are given in Table 4. The presence of an unpaired spin in the molecule led to an unrestricted calculation and different orbitals for α and β spins. The

Table 3 Bond lengths/Å and angles/° for $[(CH_3)_3ReO]_2O$, **2**, together with the corresponding distances and angles in $\{[(CH_3)_3SiCH_2]_3ReO\}_2O$ and $(CH_3)_3ReO_2$

$[(CH_3)_3ReO]_2O$						$\{[(CH_3)_3SiCH_2]_3$-$ReO\}_2O$ [a]	$(CH_3)_3ReO_2$ [b]	
Molecule **I** [c]		Molecule **II**						
Re(1)–O(1)	1.678(6)	Re(2)–O(2)	1.674(6)	Re(3)–O(3)	1.672(6)	1.671(5)	Re=O	1.703(3)
Re(1)–O(11)	1.8514(9)	Re(2)–O(23)	1.850(6)	Re(3)–O(23)	1.851(6)	1.856(5)	Re–C_{ax}	2.122(6)
Re(1)–C(11)	2.112(8)	Re(2)–C(21)	2.102(8)	Re(3)–C(31)	2.134(9)	2.132(6)	Re–C_{eq}	2.199(22)
Re(1)–C(12)	2.124(8)	Re(2)–C(22)	2.095(11)	Re(3)–C(32)	2.100(11)	2.114(6)		
Re(1)–C(13)	2.128(9)	Re(2)–C(23)	2.115(8)	Re(3)–C(33)	2.131(9)	2.133(6)		
O(1)–Re(1)–O(11)	115.6(3)	O(2)–Re(2)–O(23)	113.9(3)	O(3)–Re(3)–O(23)	114.8(3)	116.1(2)	O–Re–O	123.0(2)
O(1)–Re(1)–C(11)	109.9(3)	O(2)–Re(2)–C(21)	112.1(3)	O(3)–Re(3)–O(31)	113.5(4)	107.5(3)		
O(11)–Re(1)–C(11)	86.5(3)	O(23)–Re(2)–C(21)	86.4(3)	O(23)–Re(3)–O(31)	86.2(3)	87.3(2)		
O(1)–Re(1)–C(12)	104.4(4)	O(2)–Re(2)–C(22)	103.0(4)	O(3)–Re(3)–C(32)	103.4(4)	106.3(3)	O–Re–C_{eq}	118.5(10)
O(11)–Re(1)–C(12)	140.0(3)	O(23)–Re(2)–C(22)	143.1(4)	O(23)–Re(3)–C(32)	141.8(4)	137.6(1)		
C(11)–Re(1)–C(12)	79.4(4)	C(22)–Re(2)–C(21)	79.4(4)	C(32)–Re(3)–C(31)	79.0(4)	80.4(3)	C_{eq}–Re–C_{ax}	73.5(11)
O(1)–Re(1)–C(13)	111.2(4)	O(2)–Re(2)–C(23)	112.4(3)	O(3)–Re(3)–C(33)	112.3(4)	106.8(3)		
O(11)–Re(1)–C(13)	86.9(3)	O(23)–Re(2)–C(23)	86.4(3)	O(23)–Re(3)–C(33)	86.0(3)	87.4(2)		
C(11)–Re(1)–C(13)	137.0(4)	C(21)–Re(2)–C(23)	133.9(4)	C(31)–Re(3)–C(33)	132.5(4)	143.9(2)	C_{ax}–Re–C_{ax}	146.9(22)
C(12)–Re(1)–C(13)	78.8(4)	C(23)–Re(2)–C(22)	79.6(4)	C(33)–Re(3)–C(32)	79.0(4)	79.7(3)		
Re(1)–O(11)–Re(1a)	180.0	Re(2)–O(23)–Re(3)	178.8(4)			180.0		

[a] Values taken from the X-ray diffraction study described in ref. 21. [b] Values taken from the GED study reported in ref. 5. [c] The other atoms in molecule **I** are related to those listed by symmetry.

Table 4 Orbital energies, calculated and experimental IE, and orbital character of $(CH_3)_4ReO$, **1** [a]

	Energy, ε_i [b]		IE calc./eV			% fragment contribution				
Orbital	α	β	singlet	triplet	IE exp./eV	Re 5d	Re 6s	Re 6p	Me σ	O 2p
$9a_1$	(−2.06)	(−1.77)				43		16	12	18
9e	(−2.12)	(−1.84)				47		4	24	23
$3b_2$	−5.54	(−4.13)	8.59		8.86	83				
8e	−6.61	−6.57	9.32	9.28	9.50, 9.95	8		6	61	20
$4b_1$	−8.25	−8.11	11.03	10.90	11.2	42			39	
$8a_1$	−8.89	−8.67	11.62	11.39		7	21		6	
$1a_2$	−8.80	−8.76	11.47	11.42						
7e	−9.08	−9.04	11.79	11.77		14			2	41

[a] Only the contributions from Re 5d, 6s, 6p, O 2p and CH_3 σ SOMO are shown. [b] Parentheses indicate an unoccupied spin-orbital.

unpaired electron occupies an orbital of b_2 symmetry, d_{xy} in character, which is non-bonding with respect to the ligand set. Of particular interest are the LUMO, 9e, and the highest fully occupied orbital, 8e. Representations of these orbitals are given in Fig. 3. The fragment orbitals contributing to these MOs are the O pπ pair, the e SALCS formed from the CH_3 sp^3 hybrids, and the Re d_{xz} and d_{yz} orbitals. They mix strongly to form the occupied 7e and 8e and the unoccupied 9e orbitals. The 8e orbitals are M–C bonding and the 9e orbitals M–C antibonding. The $8a_1$ and $4b_1$ orbitals, which are also M–C bonding and occupied, are significantly more stable.

Authentication of this orbital picture may be obtained by calculation of the IE for removal of an electron from each of these orbitals, and comparison with the experimental values from the PE spectrum. The calculated and experimental IE are given in Table 4. The PE spectrum shows in its low IE region a weak band at 8.86 eV (assigned to the d ionisation, $3b_2$) followed by two bands of equal intensity at 9.50 and 9.95 eV. The first of these was originally assigned to the 8e M–C ionisation and the second to the $8a_1$ + $4b_1$ M–C ionisations. The present IE calculations suggest this assignment to be incorrect and that both bands are due to the 8e ionisation split by spin–orbit (SO) coupling. (The calculated exchange splitting is insufficient to account for the band separation and the equal intensity ratio is inconsistent with that expected from exchange splitting). The ionising orbital is calculated to have 8% d character and assuming a SO coupling constant for Re 5d of 0.2 to 0.3 eV the predicted splitting is < 0.05 eV. The most probable origin of the SO splitting comes from small contributions from the Re 5p and 6p orbitals. Similar splittings in PE bands in the spectra of OsO_4 [37] and $Os(\eta\text{-}C_5H_5)_2$ [38] have been shown to originate in a combination of core and valence p contributions to the associated orbitals. The higher M–C ionisation bands, from $8a_1$ and $4b_1$, may be associated with the shoulders perceptible on the low IE edge of the main band in the He I spectrum. The originating orbitals are thus significantly more stable than the 8e orbital, as the calculation suggests.

Matrix-isolation and photochemistry of 1

(i) IR spectrum of matrix-isolated 1. The IR spectrum of $(CH_3)_4ReO$, **1**, isolated in an argon matrix at *ca.* 16 K is depicted in Fig. 4(a). As revealed by both crystallographic and electron-diffraction [10] studies, the $(CH_3)_4ReO$ molecule conforms to C_{4v} symmetry so that the 48 vibrational fundamentals are distributed over the representations $8a_1$ + $4a_2$ + $7b_1$ + $5b_2$ + 12e. It follows that there should be 20 IR absorptions attributable to such fundamentals ($8a_1$ + 12e), although the weakness of coupling between the internal motions of the CH_3 groups is bound to result in the coincidence or near-coincidence of some transitions. The features of the observed spectrum have been assigned on the evidence (i) of the corresponding spectrum displayed by $(CD_3)_4ReO$, **1**-d_{12} [see Fig. 5(a)], (ii) of the IR properties calculated for **1** and **1**-d_{12}, and (iii) of analogies with the spectra of other rhenium oxide derivatives, *e.g.* CH_3ReO_3,[11] $(CH_3)_3ReO_2$,[5] and $OReF_4$.[13] The results are listed in Table 5.

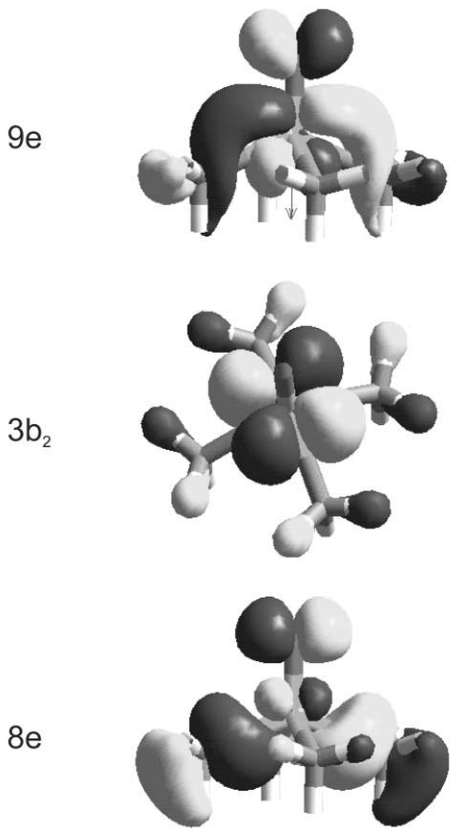

Fig. 3 Frontier orbitals of $(CH_3)_4ReO$, **1**.

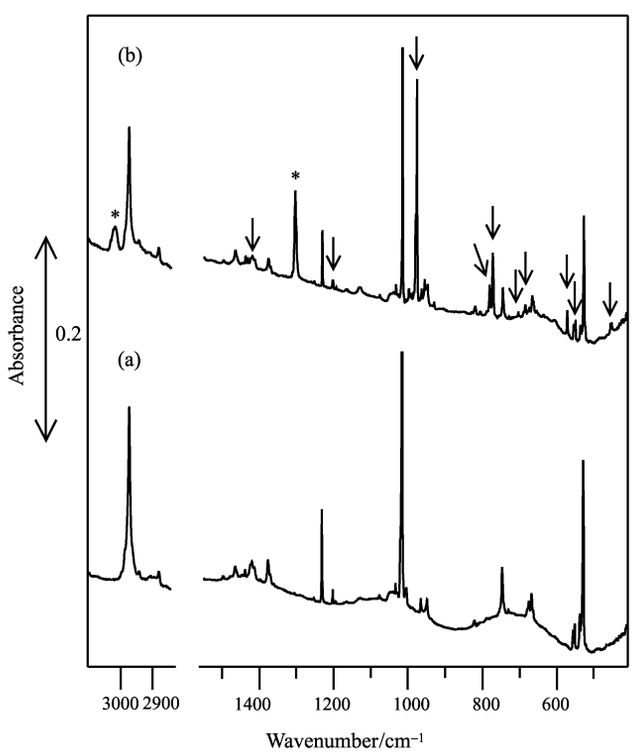

Fig. 4 IR spectra of matrix-isolated $(CH_3)_4ReO$, **1**, in an Ar matrix at 16 K (a) after deposition and (b) following broad-band UV-visible photolysis for 60 min. Bands marked * are due to methane.

Our DFT calculations reproduce satisfactorily the geometry determined experimentally for the $(CH_3)_4ReO$ molecule (see Table 2); vibrational wavenumbers and IR intensities have then been calculated for the optimum model of **1** and **1**-d_{12}. Correlation of the observed with the simulated spectrum has

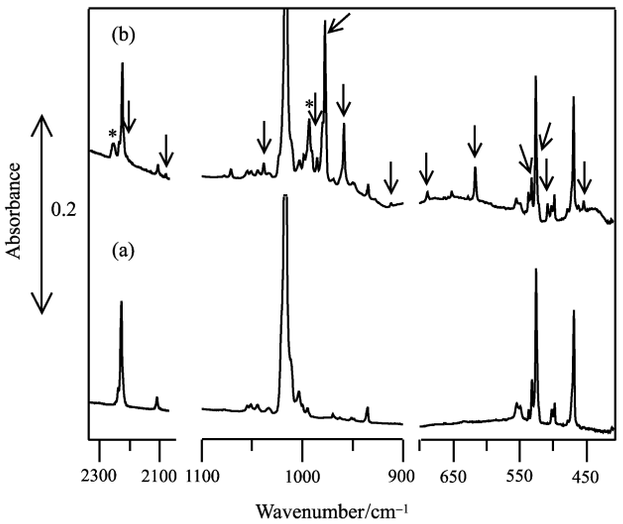

Fig. 5 IR spectra of matrix-isolated $(CD_3)_4ReO$, **1**-d_{12}, in an Ar matrix at 16 K (a) after deposition and (b) following broad-band UV-visible photolysis for 60 min. Bands marked * are due to methane.

then provided a persuasive endorsement of the vibrational assignments given in Table 6 with an r.m.s. deviation for 25 measured wavenumbers of no more than 3.67%. The most distinctive absorption occurring at 1016.3 cm^{-1} and virtually unaffected by deuteriation is readily identified with the ν(Re=O) mode. Other prominent bands include those attributable to the following motions: ν_{as}(C–H) (2975.4 cm^{-1}), $\delta_s(CH_3)$ (1231.3 cm^{-1}), and $\rho(CH_3)$ (746.1 cm^{-1}); the corresponding H/D ratios are 1.3355 : 1, 1.3168 : 1, and 1.3494 : 1, respectively. What are primarily ν(Re–C) fundamentals are then responsible for bands at 556.0/550.8 and 537.3/528.3 cm^{-1} for which H/D = 1.1060 : 1 and 1.1358 : 1, respectively. The relative intensities of the two bands imply a *trans* C–Re–C angle in the order of 140°, consistent with the values of 134–136° determined by diffraction measurements. The splitting or broadening of some bands and the observation of some very weak absorptions not listed in Table 5, for example between 1500 and 1350 cm^{-1}, were probably due to the occupation of different matrix sites, the trapping of more than one molecular conformer, and/or a reduction of local symmetry. Other very weak bands were also recognisable as arising from traces of familiar impurities, *viz.* H_2O, $[H_2O]_n$, CO and CO_2, the presence of which could be kept to a minimum but never wholly eliminated. The intensities of the bands made it quite clear, however, that the impurities played no part in the chemical changes subsequently induced by photolysis.

(ii) Effects of photolysis. Exposure of the argon matrix doped with **1** to broad-band UV-visible radiation ($200 \leq \lambda \leq 800$ nm) for 5 min resulted in the decay of the IR absorptions due to **1** with the simultaneous appearance of new absorptions having the following wavenumbers: 3024.2, 1431.6, 1311.3, 1303.9, 1203.6, 977.5, 782.4, 773.6, 704.1, 685.4, 663.6, 573.4, 553.8, 534.1 and 456.4/453.5 cm^{-1}. Continued photolysis for a period of up to 60 min caused a steady growth of these new features at the expense of the features in the original spectrum [see Fig. 4(b)]. A similar experiment with **1**-d_{12} in place of **1** yielded ultimately the IR spectrum illustrated in Fig. 5(b) which included new bands at the following wavenumbers: 2258.8, 2212.3, 2134.1, 2083.3, 1038.6, 993.4, 985.6, 977.8, 959.0, 912.5, 687.7, 616.2, 534.6, 521.7, 508.3, 461.9 and 454.3 cm^{-1}. With **1** as the precursor, the most intense product band occurred at 977.5 cm^{-1}: with **1**-d_{12} as the precursor, the most intense product band occurred at 977.8 cm^{-1}. The combination of intensity, wavenumber, and lack of response to deuteriation gives every reason to believe that this transition originates in a ν(Re=O) fundamental.

Table 5 Observed and calculated fundamental vibrational wavenumbers for **1** and **1**-d_{12} isolated in an argon matrix [a]

$(CH_3)_4ReO$		$(CD_3)_4ReO$			
exp.	calc.[b]	exp.	calc.[b]	Mode	Assignment
2975.4 (96)[c]	3034.6 (11)	2238.6/2227.9 (30)[c]	2252.3 (5)	$\nu_1(a_1)$	ν_{as}(C–H)
2887.4 (11)[c]	2940.4 (1)	2109.5 (3)	2113.0 (0)	$\nu_2(a_1)$	ν_s(C–H)
1419.4 br (11)[c]	1430.8 (19)	1055.0/1051.5 (1)	1040.8 (3)	$\nu_3(a_1)$	$\delta_{as}(CH_3)$
1231.3 (10)	1220.2 (9)	950.9 (0)	937.9 (0)	$\nu_4(a_1)$	$\delta_s(CH_3)$
1016.3 (100)	1000.6 (100)	1016.8 (100)	1000.3 (100)	$\nu_5(a_1)$	ν(Re=O)
746.1 (13)	726.3 (6)	552.2/549.8 (5)	570.9 (2)	$\nu_6(a_1)$	$\rho(CH_3)$
556.0/550.8 (5)	539.4 (5)	502.5/498.2 (3)	489.6 (4)	$\nu_7(a_1)$	ν(Re–C)
	214.0 (1)		185.0 (1)	$\nu_8(a_1)$	$\delta_s(ReC_4)$
	3022.8 (0)		2246.6 (0)	$\nu_9(a_2)$	ν_{as}(C–H)
	1371.5 (0)		996.4 (0)	$\nu_{10}(a_2)$	$\delta_{as}(CH_3)$
	746.5 (0)		558.4 (0)	$\nu_{11}(a_2)$	$\rho(CH_3)$
	12.4 (0)		15.1 (0)	$\nu_{12}(a_2)$	CH_3 twist
	3019.8 (0)		2242.0 (0)	$\nu_{13}(b_1)$	ν_{as}(C–H)
	2934.1 (0)		2107.4 (0)	$\nu_{14}(b_1)$	ν_s(C–H)
	1387.0 (0)		1009.4 (0)	$\nu_{15}(b_1)$	$\delta_{as}(CH_3)$
	1176.1 (0)		914.0 (0)	$\nu_{16}(b_1)$	$\delta_s(CH_3)$
	717.3 (0)		554.6 (0)	$\nu_{17}(b_1)$	$\rho(CH_3)$
	471.5 (0)		424.9 (0)	$\nu_{18}(b_1)$	ν(Re–C)
	105.9 (0)		91.9 (0)	$\nu_{19}(b_1)$	δ(Re–C)
	3031.5 (0)		2250.5 (0)	$\nu_{20}(b_2)$	ν_{as}(C–H)
	1405.3 (0)		1022.9 (0)	$\nu_{21}(b_2)$	$\delta_{as}(CH_3)$
	760.3 (0)		574.2 (0)	$\nu_{22}(b_2)$	$\rho(CH_3)$
	326.1 (0)		280.6 (0)	$\nu_{23}(b_2)$	δ(Re–C)
	193.7 (0)		141.1 (0)	$\nu_{24}(b_2)$	CH_3 twist
2975.4 (96)[c]	3030.2 (46)	2238.6/2227.9 (30)[c]	2249.2 (17)	$\nu_{25}(e)$	ν_{as}(C–H)
2975.4 (96)[c]	3023.2 (1)	2238.6/2227.9 (30)[c]	2243.7 (0)	$\nu_{26}(e)$	
2887.4 (11)[c]	2937.8 (21)	2109.5 (3)[c]	2110.5 (6)	$\nu_{27}(e)$	ν_s(C–H)
1419.4 br (11)[c]	1403.9 (8)	1044.8 (1)	1022.6 (4)	$\nu_{28}(e)$	$\delta_{as}(CH_3)$
1376.4 (10)	1388.1 (6)	1033.8 (1)	1010.2 (5)	$\nu_{29}(e)$	
1202.3 (1)	1191.9 (1)	934.9 (1)	922.5 (5)	$\nu_{30}(e)$	$\delta_s(CH_3)$
746.1 (13)	727.4 (7)	532.2 (4)	541.1 (4)	$\nu_{31}(e)$	$\rho(CH_3)$
674.3 (5)	659.9 (6)	526.1 (17)	517.4 (14)	$\nu_{32}(e)$	
537.3/528.3 (43)	509.1 (38)	469.1 (14)	452.5 (17)	$\nu_{33}(e)$	ν(Re–C)
	217.0 (0)		208.0 (0)	$\nu_{34}(e)$	Re–O wag
	196.8 (9)		174.3 (5)	$\nu_{35}(e)$	δ(ReC_4)
	142.3 (0)		105.7 (0)	$\nu_{36}(e)$	CH_3 twist

[a] Wavenumbers in cm^{-1}; intensities (in parentheses) normalised to that of the most intense band set equal to 100. br = broad. [b] Details of the ADF calculations are given in the text. [c] A single observed band encompasses a number of calculated bands of similar wavenumber.

Solutions of **1** in n-hexane are reported [36] to display a UV-visible absorption spectrum comprising four bands, these being centred at 285, 341, 460 and 565 nm. Experiments were therefore attempted with photolysing radiation restricted to particular wavelengths to see whether the course of the photochemical change could be influenced in this way. Under the action of visible light with $\lambda \geq 400$ nm, however, matrix-isolated **1** suffered no significant change, on the evidence of its IR spectrum. Broad-band UV light with $\lambda = 200$–400 nm was observed to bring about the same changes as did broad-band UV-visible light, but at a much reduced rate. The optimum conditions were therefore achieved with minimal filtering of the photolysing radiation, with no sign of photochemical selectivity. Warming the photolysed matrices at temperatures up to 35 K failed to elicit any significant change in the IR spectrum.

Careful analysis of the IR spectra of the irradiated deposits leads us to conclude that two photoproducts are formed, namely CH_4 and the novel methylidene derivative $H_2C{=}Re(O)(CH_3)_2$, **3**. The identities of these products have been established by the wavenumber and intensity patterns, by the response of the patterns to perdeuteriation of the precursor, and, in the case of **3**, by reference to the IR spectra simulated by DFT calculations. In the following account wavenumbers given in parentheses relate to the perdeuteriated version of the molecule in question.

Recognition that the two relatively broad bands at 3024.2 (2258.8) and 1303.9 (993.4) cm^{-1} were carried by CH_4 (CD_4) has been crucial to working out the fate of **1** on broad-band UV-visible photolysis. The wavenumbers and relative intensities leave little doubt that these correspond to the t_2 fundamentals of CH_4 (CD_4), in keeping with the IR spectra reported elsewhere [39] for the matrix-isolated molecule. That the wavenumbers recorded here differ by up to 10 cm^{-1} from those reported previously suggests some perturbation of the CH_4 formed in our experiments under the action of other guest species in the matrix environment. The production of CH_4 from $(CH_3)_4ReO$ then gives strong circumstantial grounds for believing that the complementary metal-containing product, **3**, is the methylidene derivative $H_2C{=}Re(O)(CH_3)_2$.

Certainly the prominent IR absorption at 977.5 cm^{-1} supports the presence in **3** of an Re=O fragment, what is presumed to be the ν(Re=O) mode occurring 38.8 cm^{-1} to low wavenumber of the corresponding mode of $(CH_3)_4ReO$.

In addition, the presence of an $Re{=}CH_2$ unit in **3** is signalled by the appearance of IR bands at 1311.3, 782.4, 773.6, 573.4, and 456.4/453.5 cm^{-1} which we associate with the modes detailed in Table 6. Guidance in the interpretation of these features is to be found in the spectra reported by Margrave and co-workers for the simple methylidene derivatives $M{=}CH_2$ where M=Cr,[12a] Mn,[12b] Fe,[12c] Co,[12d] Ni,[12e] or Cu,[12f] which have been trapped in solid argon following the reaction of the appropriate metal atom M with diazomethane. Further parallels may also be drawn with the spectrum of $H_2C{=}Re(O)_2OH$ formed in an argon matrix by photoisomerisation of CH_3ReO_3.[11] On this basis, the shoulder at 1311.3 cm^{-1} in the spectrum of **3** is most plausibly identified with the $\delta(CH_2)$ mode, an assignment supported by its shift on perdeuteriation to 1038.6 cm^{-1} (H/D = 1.2626 : 1); the corresponding features of $H_2C{=}Re(O)_2OH$ and $D_2C{=}Re(O)_2OD$ occur at 1320.9 and

Table 6 Observed and calculated fundamental vibrational wavenumbers for **3** and **3**-d_8 isolated in an argon matrix [a]

$H_2CRe(O)(CH_3)_2$		$D_2CRe(O)(CD_3)_2$			
exp.	calc.[b]	exp.	calc.[b]	Mode	Assignment
	3079.7 (0)		2291.3 (1)	$\nu_1(a')$	$\nu_{as}(CH_2)$
	3009.7 (2)	2212.3 (1)[c]	2233.4 (1)	$\nu_2(a')$	$\nu_{as}(CH_3)$
	3004.4 (8)	2212.3 (1)[c]	2229.8 (4)	$\nu_3(a')$	
	2951.2 (1)	2134.1 (1)	2148.7 (1)	$\nu_4(a')$	$\nu_s(CH_2)$
	2923.5 (4)	2083.3 (4)	2100.7 (1)	$\nu_5(a')$	$\nu_s(CH_3)$
1431.6 (3)	1398.2 (12)		1016.2 (4)	$\nu_6(a')$	$\delta_{as}(CH_3)$
	1380.8 (2)		1003.2 (2)	$\nu_7(a')$	
1311.3 sh	1307.7 (4)	1038.6 (5)	1032.5 (8)	$\nu_8(a')$	$\delta(CH_2)$
	1187.0 (0)	959.0 (12)	931.3 (0)	$\nu_9(a')$	$\delta_s(CH_3)$
977.5 (100)	966.7 (100)	977.8 (100)	966.0 (100)	$\nu_{10}(a')$	ν(Re=O)
782.4 (9)	790.0 (16)	687.7 (6)	693.2 (9)	$\nu_{11}(a')$	ν(Re=C)
704.1 (2)	710.2 (2)		549.9 (0)	$\nu_{12}(a')$	$\rho(CH_3)$
685.4 br (6)[c]	694.1 (4)	534.6 sh	531.2 (3)	$\nu_{13}(a')$	
573.4 (8)	578.3 (4)	454.3 (4)	445.6 (3)	$\nu_{14}(a')$	CH_2 scissor
534.1 sh	527.6 (11)	508.3 (8)	499.6 (8)	$\nu_{15}(a')$	ν(Re–C)
	224.7 (1)		201.2 (1)	$\nu_{16}(a')$	Re–O wag
	197.0 (1)		168.9 (1)	$\nu_{17}(a')$	CH_2 wag
	164.0 (0)		120.2 (0)	$\nu_{18}(a')$	CH_3 twist
	110.0 (0)		96.8 (0)	$\nu_{19}(a')$	δ(Re–C)
	3009.3 (7)	2212.3 (1)[c]	2232.9 (3)	$\nu_{20}(a'')$	$\nu_{as}(CH_3)$
	3002.0 (0)	2212.3 (1)[c]	2227.6 (0)	$\nu_{21}(a'')$	
	2921.4 (1)	2083.3 (4)	2098.8 (0)	$\nu_{22}(a'')$	$\nu_s(CH_3)$
	1393.3 (0)		1013.3 (0)	$\nu_{23}(a'')$	$\delta_{as}(CH_3)$
	1373.5 (5)	985.6 (4)	998.8 (3)	$\nu_{24}(a'')$	
1203.6 (4)	1196.8 (3)	912.5 (2)	926.7 (1)	$\nu_{25}(a'')$	$\delta_s(CH_3)$
773.6 (32)	764.3 (35)	616.2 (23)	608.4 (21)	$\nu_{26}(a'')$	$\rho(CH_2)$
685.4 br (6)[c]	685.5 (3)		525.5 (6)	$\nu_{27}(a'')$	$\rho(CH_3)$
663.6 sh	660.8 (5)	521.7 sh	520.4 (3)	$\nu_{28}(a'')$	
553.8[d]	541.5 (8)	461.9 (1)	462.5 (3)	$\nu_{29}(a'')$	ν(Re–C)
456.4/453.5(9)	447.2 (10)		329.8 (3)	$\nu_{30}(a'')$	CH_2 twist
	203.2 (1)		186.7 (1)	$\nu_{31}(a'')$	Re–O wag
	179.0 (0)		159.5 (0)	$\nu_{32}(a'')$	CH_2 wag
	167.7 (0)		119.7 (0)	$\nu_{33}(a'')$	CH_3 twist

[a] Wavenumbers in cm^{-1}; intensities (in parentheses) normalised to that of the most intense band set equal to 100. br = broad, sh = shoulder. [b] Details of the ADF calculations are given in the text. [c] A single observed band encompasses a number of calculated bands of similar wavenumber. [d] A weak band on the flank of a much stronger feature, making it impossible to measure accurately the intensity.

1009.9 cm^{-1}, respectively. Next in order of decreasing wavenumber come the bands at 782.4 and 773.6 cm^{-1} which can be identified with the ν(Re=C) and $\rho(CH_2)$ fundamentals, respectively. These shift to 687.7 and 616.2 cm^{-1} on perdeuteriation, giving H/D = 1.1377 : 1 and 1.2554 : 1. Attributable to the CH_2 scissoring and wagging modes are the two absorptions at lower wavenumber, *viz.* 573.4 and 456.4/453.5 cm^{-1}. Perdeuteriation causes the first to move, as expected, to 454.3 cm^{-1} (H/D = 1.2622 : 1), whereas the counterpart to the second could not be observed at wavenumbers > 400 cm^{-1} (the low-energy threshold of the present measurements).

Evidence that **3** contains an $Re(CH_3)_2$ moiety is less immediately obvious. None of the relevant fundamentals is likely to be particularly intense in IR absorption, and this problem is compounded by the circumstance that all are likely to occur at wavenumbers close to the corresponding modes of the precursor **1**, rendering the relevant bands of **3** vulnerable to masking by those due to unchanged **1**. For these reasons, presumably, it was not possible to detect any signals from **3** that could be associated with ν(C–H) modes, although the deuteriated version of **3** did show features at 2212.3, 2134.1 and 2083.3 cm^{-1} that can reasonably be attributed to ν(C–D) modes of CD_3 groups. The band at 1431.6 cm^{-1} is plainly a candidate for an antisymmetric $\delta(CH_3)$ vibration, just as the peak at 1203.6 cm^{-1} is the obvious choice for a symmetric $\delta(CH_3)$ vibration. Weak bands in the region 660–710 cm^{-1} have the right credentials to be associated with $\rho(CH_3)$ fundamentals, while the band at 553.8 cm^{-1}, along with a shoulder at 524.1 cm^{-1}, represent the two ν(Re–C) vibrations.

The preceding analysis is therefore wholly consistent with the belief that **3** is the methylidene complex $H_2C{=}Re(O)(CH_3)_2$ formed by elimination of CH_4 from $(CH_3)_4ReO$ (eqn. (1)). DFT calculations find an equilibrium geometry for such a complex conforming to C_s symmetry (see Fig. 6), with pseudotetrahedral

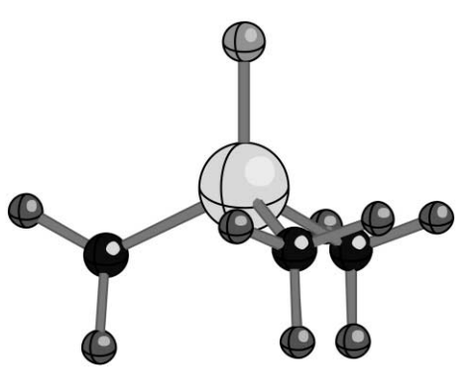

Fig. 6 Calculated structure for $H_2C{=}Re(O)(CH_3)_2$, **3**.

coordination of the metal atom and O=Re=C and C–Re–C bond angles of 116 and 109°, respectively; the CH_2 group lies in the symmetry plane of the molecule. The enthalpy change for reaction (1) is estimated to be 13 kJ mol^{-1}. The vibrational wavenumbers computed from the DFT-based force field for the isotopomers $H_2C{=}Re(O)(CH_3)_2$, **3**, and $D_2C{=}Re(O)(CD_3)_2$, **3**-d_8, are listed, together with predicted IR intensities, in Table 6, while the observed and calculated IR spectra are compared in Fig. 7. The properties simulated in this way are thus found to be in generally close agreement with the experimental results. For example, the 29 wavenumbers measured for **3** and **3**-d_8 can be matched by calculation with an r.m.s. deviation of 2.02%. The

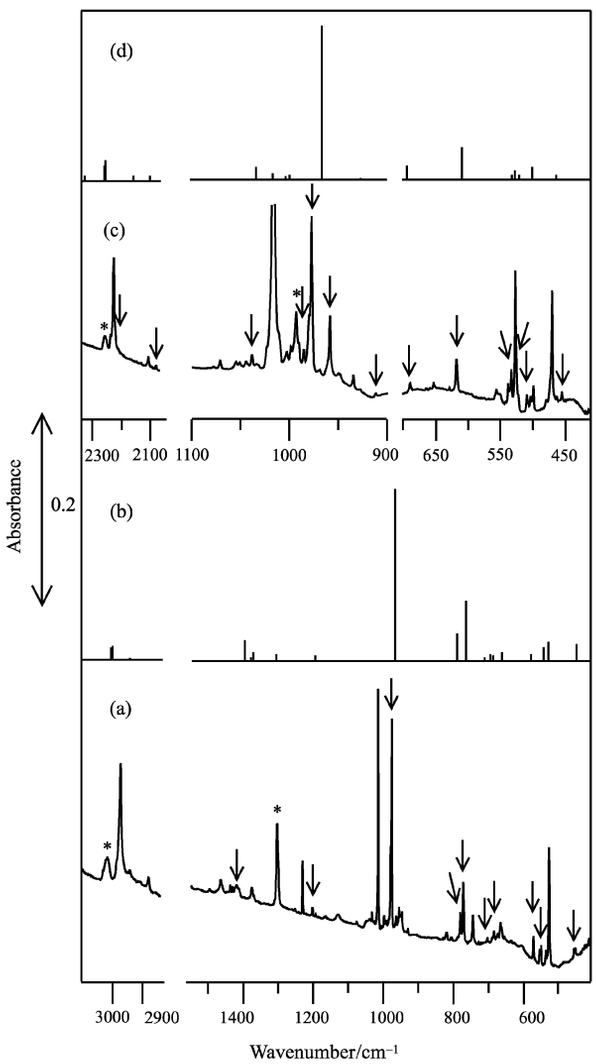

Fig. 7 Observed (a) and calculated (b) IR spectrum of H_2C=$Re(O)(CH_3)_2$, **3**. Observed (c) and calculated (d) IR spectrum of D_2C=$Re(O)(CD_3)_2$, **3**-d_8. The arrows in (a) and (c) indicate bands assigned to **3** and **3**-d_8, respectively. Bands marked * are due to methane.

failure to detect the remaining fundamental transitions can then be perfectly well understood in terms of one or more of the following factors: (i) inherently low intensity; (ii) masking by the absorptions of CH_4 or the unchanged precursor; and (iii) falling outside the limits of detection of the present measurements.

(iii) Reaction mechanism. The results reported and analysed in the preceding section seem to leave little doubt that broad-band UV-visible photolysis of matrix-isolated $(CH_3)_4ReO$ brings about the formation of the methylidene–rhenium(VI) species H_2C=$Re(O)(CH_3)_2$ with the elimination of CH_4 (eqn. (1)). It is a consequence of the conditions of our experiments, where the precursor is trapped at high dilution (*ca.* 1 : 1000), that any change must initially be unimolecular in nature, and that the CH_4 extruded must originate solely from the parent molecule.

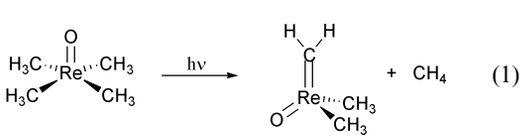

(1)

Examples of the photochemical generation of alkylidene-rhenium from alkyl-rhenium derivatives already exist. It was by photolysis of a solution of $[(CH_3)_3CCH_2]_3ReO_2$ in pyridine that Hoffman *et al.* succeeded in producing the first alkylidene derivative of a rhenium(VII) oxide, *viz.* $[(CH_3)_3CHC][(CH_3)_3CCH_2]ReO_2$, with concomitant loss of neopentane.[40] More recent studies of matrix-isolated trimethyldioxorhenium(VII), $(CH_3)_3ReO_2$, have also revealed that broad-band UV-visible irradiation results in a similar primary reaction, now with the formation of H_2C=$Re(CH_3)O_2$ and CH_4.[41] On the other hand, this pathway exists only where the precursor contains two or more alkyl ligands, and in the case of methyltrioxorhenium(VII), photolysis under similar conditions has been shown[11] to induce the formation of a methylidene–rhenium derivative, but by tautomerisation rather than elimination (eqn. (2)). Although such tautomerisation is also open to $(CH_3)_4ReO$, to give H_2C=$Re(CH_3)_3(OH)$, the identification of CH_4 as a product and the failure to pick up any spectroscopic sign of an Re–OH group[11] give us every reason to believe that this route loses out to methane elimination as the preferred means of hydrogen abstraction.

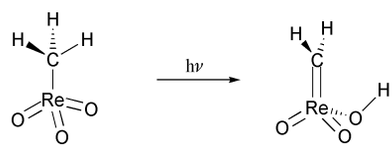

(2)

There exist, in principle, three possible routes leading from **1** to **3** + CH_4, as set out in Scheme 1.

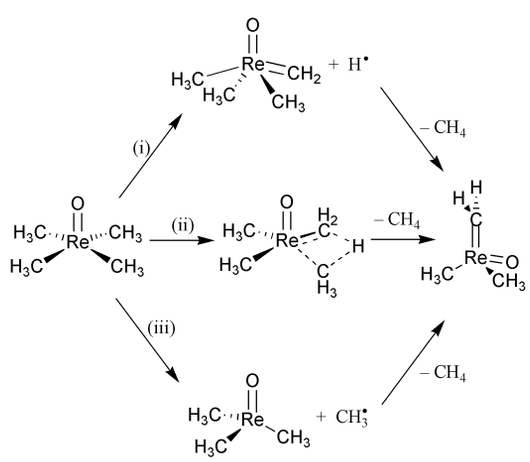

Scheme 1 Possible mechanisms for the photoconversion of **1** to **3** in an Ar matrix at 16 K.

(*i*) The first pathway involves fission of a C–H bond in a methyl group of **1** with the formation of an H• atom and the rhenium(VII) compound H_2C=$Re(CH_3)_3O$. The H• atom could then engage in abstraction of a CH_3 group to form CH_4 and **3**. However, cleavage of a C–H bond as a primary event seems improbable under the conditions of our experiments, and it is unlikely too that the H• atoms formed in this process would be retained efficiently by the matrix cage. On the evidence of previous studies,[42] H• atoms are quite mobile in argon matrices and might be expected in large part to migrate away from the site of their formation.

(*ii*) An alternative requires extraction of one of the hydrogens of a methyl group of **1** by an adjacent methyl group *via* a four-centred transition state. The structure and spectroscopic properties of **1** give no hint of a close $CH_3 \cdots CH_3$ approach or of significant vibrational perturbation or pliability of the Re–CH_3 moieties, at least in the electronic ground state of the molecule. Although there may be an appreciable change of geometry in one or more of its electronically excited states, we lack positive evidence favouring such an intramolecular mechanism.

(*iii*) Perhaps the most likely route to **3** would therefore seem to depend on homolysis of an Re–CH_3 bond, as is believed to

be the primary photoprocess occurring on UV irradiation of CH_3ReO_3.[10,43] The first step would then be the formation of $CH_3^{\bullet}$ and the rhenium(v) compound $(CH_3)_3ReO$. The $CH_3^{\bullet}$ radical then engages in H atom abstraction from a neighbouring CH_3 substituent of $(CH_3)_3ReO$, thereby producing CH_4 and reoxidising the metal centre to the +6 state in **3**. Such photochemical α-H abstraction is not without precedent. For example, Rettig *et al.* have described[44] the formation of $[(P_2N_2)Ta(CH_2)CH_3]$ and CH_4 by UV irradiation of $[(P_2N_2)Ta(CH_3)_3]$ in hexane solution at room temperature {P_2N_2 = $PhP[CH_2SiMe_2NSiMe_2CH_2]_2PPh$}. A similar mechanism involving H atom abstraction by a methyl radical is also thought to operate in the photoelimination of CH_4 from the trigonal bipyramidal complex $[TaX_2(CH_3)_3]$ (X = 2,6-$Bu^t_2C_6H_3O$),[45] although it has also been suggested that this may proceed by a more concerted reaction mechanism involving a four-centred transition state [not necessarily unlike that in (ii)]. As between dissociation + abstraction or concerted elimination, our experiments are unable to make any very meaningful distinction. Admittedly, the IR spectra gave no hint of bands attributable to free $CH_3^{\bullet}$ or $CD_3^{\bullet}$ radicals[46] which might have escaped the second stage of the reaction, but the radicals may well be strongly perturbed by the adjacent $(CH_3)_3ReO$ molecules, and so this scarcely amounts to a ringing endorsement of a concerted mechanism.

Attempts to model the reaction pathways (i)–(iii), starting from **1** in its ground electronic state, met with only moderate success. Decreasing stepwise the C ··· H distance between a methyl hydrogen and an adjacent C to simulate pathway (ii), led to the expected products of methane and the oxy-carbene but the energy was discontinuous and a transition state was not identified (max 2.20 eV). Modelling pathway (i) by increasing stepwise a C–H bond length gave identical products and also a discontinuous energy (max 3.09 eV). The energy difference between $(CH_3)_4ReO$ and a combination of $(CH_3)_3(CH_2)ReO$ and a H atom is calculated to be 439 kJ mol^{-1}. Stepping the Re–C distance, in order to model (iii), gave a smoothly increasing energy and the formation of a planar methyl group and a tetrahedral $ReOMe_3$. The energy difference for forming these two isolated species (the latter with spin 1) is 221 kJ mol^{-1}.

It is clear that the matrix reaction affording **3** is photochemically initiated by broad-band UV irradiation with λ = 200–400 nm. The UV-vis spectrum of **3** is reported as having two strong complex bands with identifiable features at 565, 460, 341 and 285 nm (2.19, 2.70, 3.63 and 4.35 eV, respectively).[36] Thus UV irradiation will excite the lower two transitions. A rough estimate of excitation energies may be made from the present calculation on the basis of Koopmans′ approximation. A more definite assignment lies outside the scope of the current work. The energies of the lower unoccupied orbitals are given in Table 4. These suggest that possible transitions are $3b_2 \longrightarrow 9e$, and $8e \longrightarrow 3b_2$. In C_{4v} symmetry both these transitions are dipole-allowed whereas $3b_2 \longrightarrow 9a_1$ is dipole-forbidden. Excitation from the $3b_2$ orbital to the 9e orbital would involve promotion of a non-bonding electron to an orbital which is M–C anti-bonding. The calculated orbital energy difference is 3.42 eV. Alternatively, promotion of an electron from the 8e M–C bonding orbital to the $3b_2$ orbital (an energy difference of 2.44 eV) should also have the effect of weakening the M–C bond. Such findings support the conclusion that the reaction proceeds by photochemical initiation of M–CH_3 bond cleavage, followed by abstraction of an H atom, as represented in pathway (iii).

Conclusions

The structures determined for single crystals of $(CH_3)_4ReO$, **1**, and the related binuclear complex $[(CH_3)_3Re(O)]_2O$, **2**, feature square-pyramidal coordination of the metal centres and confirm that the former retains a discrete molecular form in the solid state, with dimensions very similar to those of the gaseous molecule.[10] The production of **2** from **1**, which has not been reported previously, probably involves a slow reaction with aerial moisture (inadvertently admitted in this case) proceeding through the formation of an initial complex with **1**, followed by the elimination of CH_4 to give $(CH_3)_3Re(O)OH$, two molecules of which then condense together to afford **2**, as in Scheme 2.

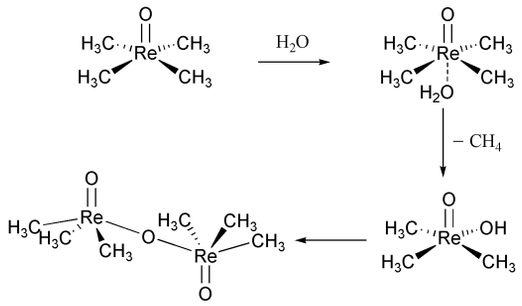

Scheme 2 Possible reactions leading to the formation of **2**.

However, dioxygen may play an active part since Beattie and Jones[47] have shown that exposure to dry air ultimately converts $(CH_3)_4ReO$ to CH_3ReO_3. Hence it is clear that O_2, like NO,[7] is capable of oxidising Re(VI) to Re(VII), and **2** is a potential intermediate in this path. There is clearly scope for further investigation of this and other reactions of **1**.

DFT calculations have been used to investigate the electronic structure of **1**. In the light of these calculations the PE spectrum of $(CH_3)_4ReO$ has been reassigned.

Isolation of **1** in a solid argon matrix at *ca.* 16 K and exposure to radiation spanning the wavelengths 200–800 nm results in the elimination of CH_4 and the formation of the novel methylidene–rhenium(VI) compound $H_2C{=}Re(O)(CH_3)_2$, **3**, the properties of which have been characterised by IR measurements on the normal and perdeuteriated isotopomers and on the basis of DFT calculations. Hence **1** differs from methyltrioxorhenium, CH_3ReO_3, which rearranges to $H_2C{=}Re(O)_2OH$ in these circumstances.[11] Although access to the methylidene compound **3** might suggest that **1** has the potential to promote olefin metathesis, the elimination of CH_4 in what is almost certainly an irreversible change holds out little prospect for useful catalytic action to match that of CH_3ReO_3,[10,48] unless the compound can be modified so as to encourage tautomerisation in preference to methane elimination.

Acknowledgements

We thank the EPSRC for support of this research, including the funding of an Advanced Fellowship (to T.M.G.) and a research studentship (to L.J.M.). Part of this work has been carried out using the computational resources of a DEC8400 multiprocessor cluster (Columbus/Magellan), provided by the UK Computational Chemistry Facility at Rutherford Appleton Laboratory and part using the facilities of the Oxford Supercomputing Centre.

References

1 K. Mertis, J. F. Gibson and G. Wilkinson, *J. Chem. Soc., Chem. Commun.*, 1974, 93.
2 W. A. Herrmann, *J. Organomet. Chem.*, 1995, **500**, 149.
3 C. C. Romão, F. E. Kühn and W. A. Herrmann, *Chem. Rev.*, 1997, **97**, 3197.
4 W. A. Herrmann, C. C. Romão, R. W. Fischer, P. Kiprof and C. de Merić de Bellefon, *Angew. Chem., Int. Ed. Engl.*, 1991, **30**, 185.
5 A. Haaland, W. Scherer, H. V. Volden, H. P. Verne, O. Gropen, G. S. McGrady, A. J. Downs, G. Dierker, W. A. Herrmann, P. W. Roesky and M. R. Geisberger, *Organometallics*, 2000, **19**, 22.
6 W. A. Herrmann, J. G. Kuchler, J. K. Felixberger, E. Herdtweck and W. Wagner, *Angew. Chem., Int. Ed. Engl.*, 1988, **27**, 394.
7 K. Mertis, D. H. Williamson and G. Wilkinson, *J. Chem. Soc., Dalton Trans.*, 1975, 607.

8 L. Galyer, K. Mertis and G. Wilkinson, *J. Organomet. Chem.*, 1975, **85**, C37.
9 J. C. Green, D. R. Lloyd, L. Gayler, K. Mertis and G. Wilkinson, *J. Chem. Soc., Dalton Trans.*, 1978, 1403.
10 A. Haaland, H. P. Verne, H. V. Volden, W. A. Herrmann and P. Kiprof, *J. Mol. Struct.*, 1995, **352/353**, 153.
11 L. J. Morris, A. J. Downs, T. M. Greene, G. S. McGrady, W. A. Herrmann, P. Sirsch, W. Scherer and O. Gropen, *Organometallics*, 2001, **20**, 2344.
12 (*a*) W. E. Billups, S.-C. Chang, R. H. Hauge and J. L. Margrave, *Inorg. Chem.*, 1993, **32**, 1529; (*b*) W. E. Billups, S.-C. Chang, J. L. Margrave and R. H. Hauge, *Organometallics*, 1999, **18**, 3551; (*c*) S.-C. Chang, R. H. Hauge, Z. H. Kafafi, J. L. Margrave and W. E. Billups, *J. Am. Chem. Soc.*, 1988, **110**, 7975; (*d*) W. E. Billups, S.-C. Chang, R. H. Hauge and J. L. Margrave, *J. Am. Chem. Soc.*, 1995, **117**, 1387; (*e*) S.-C. Chang, R. H. Hauge, Z. H. Kafafi, J. L. Margrave and W. E. Billups, *Inorg. Chem.*, 1990, **29**, 4373; (*f*) S.-C. Chang, Z. H. Kafafi, R. H. Hauge, W. E. Billups and J. L. Margrave, *J. Am. Chem. Soc.*, 1987, **109**, 4508.
13 A. K. Brisdon, J. H. Holloway, E. G. Hope, P. J. Townson, W. Levason and J. S. Ogden, *J. Chem. Soc., Dalton Trans.*, 1991, 3127.
14 R. J. Cernik, W. Clegg, C. R. A. Catlow, G. Bushnell-Wye, J. V. Flaherty, G. N. Greaves, M. Hamichi, I. Burrows, D. J. Taylor and S. J. Teat, A New High Flux Chemical and Materials Crystallography Station at the SRS Daresbury: Part 1 Design, Commissioning and Test Results, *J. Synchrotron Rad.*, 1997, **4**, 286.
15 SADABS, Bruker Analytical X-ray Instruments, Madison, WI, USA.
16 L. J. Farrugia, FPRIME, incorporated into the WinGX program system, University of Glasgow, Glasgow, 1998.
17 G. M. Sheldrick, SHELXTL, University of Göttingen, Göttingen, Germany, 1997.
18 D. J. Watkin, C. K. Prout, J. R. Carruthers, P. W. Betteridge and R. I. Cooper, CRYSTALS, Issue 11. Chemical Crystallography Laboratory, University of Oxford, Oxford, 2000.
19 D. J. Watkin, *Acta Crystallogr.*, 1994, **A50**, 411.
20 P. T. Beurskens, G. Beurskens, W. P. Bosman, R. de Gelder, S. Garcia-Granda, R. O. Gould, R. Israel and J. M. M. Smits, DIRDIF96 program system, Crystallography Laboratory, University of Nijmegen, The Netherlands, 1996.
21 P. Stavropoulos, P. G. Edwards, G. Wilkinson, M. Motevalli, K. M. A. Malik and M. B. Hursthouse, *J. Chem. Soc., Dalton Trans.*, 1985, 2167.
22 H.-J. Himmel, A. J. Downs, T. M. Greene and L. Andrews, *Organometallics*, 2000, **19**, 1060.
23 C. Fonseca Guerra, J. G. Snijders, G. te Velde and E. J. Baerends, *Theor. Chem. Acc.*, 1998, **99**, 391; S. J. A. van Gisbergen, J. G. Snijders and E. J. Baerends, *Comput. Phys. Commun.*, 1999, **118**, 119.
24 S. H. Vosko, L. Wilk and M. Nusair, *Can. J. Phys.*, 1980, **58**, 1200.
25 A. D. Becke, *Phys. Rev.*, 1988, **A38**, 2398.
26 J. P. Perdew, *Phys. Rev.*, 1986, **B33**, 8822.
27 J. P. Perdew, *Phys. Rev.*, 1986, **B34**, 7046.
28 A. J. Edwards, *J. Chem. Soc., Dalton Trans.*, 1972, 582.
29 K. Hagen, R. J. Hobson, D. A. Rice and N. Turp, *J. Mol. Struct.*, 1985, **128**, 33.
30 H. Hess and H. Hartung, *Z. Anorg. Allg. Chem.*, 1966, **344**, 157.
31 W. A. Herrmann, W. Scherer, R. W. Fischer, J. Blümel, M. Kleine, W. Mertin, R. Gruehn, J. Mink, H. Boysen, C. C. Wilson, R. M. Ibberson, L. Bachmann and M. Mattner, *J. Am. Chem. Soc.*, 1995, **117**, 3231.
32 V. Pfennig and K. Seppelt, *Science*, 1996, **271**, 626; S. Kleinhenz, V. Pfennig and K. Seppelt, *Chem. Eur. J.*, 1998, **4**, 1687.
33 K. Rypdal, W. A. Herrmann, S. J. Eder, R. W. Albach, P. Watzlowik, H. Bock and B. Solouki, *Organometallics*, 1991, **10**, 1331.
34 C. R. Pulham, A. Haaland, A. Hammel, K. Rypdal, H. P. Verne and H. V. Volden, *Angew. Chem., Int. Ed. Engl.*, 1992, **31**, 1464.
35 A. Haaland, A. Hammel, K. Rypdal and H. V. Volden, *J. Am. Chem. Soc.*, 1990, **112**, 4547.
36 J. F. Gibson, K. Mertis and G. Wilkinson, *J. Chem. Soc., Dalton Trans.*, 1975, 1093.
37 B. E. Bursten, J. C. Green and N. Kaltsoyannis, *Inorg. Chem.*, 1994, **33**, 2315.
38 A. Bähr, G. Cooper, J. C. Green, K. A. Longley, M. Lovell-Smith and G. S. McGrady, *Chem. Phys.*, 1996, **203**, 223.
39 F. H. Frayer and G. E. Ewing, *J. Chem. Phys.*, 1968, **48**, 781; A. Chamberland, R. Belzile and A. Cabana, *Can. J. Chem.*, 1970, **48**, 1129.
40 S. Cai, D. M. Hoffman and D. A. Wierda, *J. Chem. Soc., Chem. Commun.*, 1988, 1489.
41 A. J. Downs, G. Dierker, J. C. Green, T. M. Greene, G. S. McGrady, L. J. Morris, W. Scherer and P. Sirsch, *J. Chem. Soc., Dalton Trans.*, 2002, DOI: 10.1039/b204238j.
42 V. E. Bondybey, M. Räsänen and A. Lammers, *Annu. Rep. Prog. Chem., Sect. C*, 1999, **95**, 331.
43 H. Kunkely, T. Türk, C. Teixeira, C. de Merić de Bellefon, W. A. Herrmann and A. Vogler, *Organometallics*, 1991, **10**, 2090.
44 M. D. Fryzuk, S. A. Johnson and S. J. Rettig, *Organometallics*, 1999, **18**, 4059.
45 L. R. Chamberlain and I. P. Rothwell, *J. Chem. Soc., Dalton Trans.*, 1987, 163.
46 D. E. Milligan and M. E. Jacox, *J. Chem. Phys.*, 1967, **47**, 5146.
47 I. R. Beattie and P. J. Jones, *Inorg. Chem.*, 1979, **18**, 2318.
48 W. A. Herrmann, W. Wagner, U. N. Flessner, U. Volkhardt and H. Komber, *Angew. Chem., Int. Ed. Engl.*, 1991, **30**, 1636.